Microfabricated Coupled-Inductors for DC-DC Converters for Microprocessor Power Delivery

S. Prabhakaran
T. O'Donnell
C. O'Mathuna
C. R. Sullivan

Found in *IEEE Power Electronics Specialists Conference,* June 2004, pp. 4467–4472.

Microfabricated Coupled Inductors for DC-DC Converters for Microprocessor Power Delivery

Satish Prabhakaran, Charles.R. Sullivan
Thayer School of Engineering, Dartmouth College
8000 Cummings Hall
Hanover, NH, USA
Email: satish.prabhakaran@dartmouth.edu

Terence O'Donnell, Magali Brunet, Saibal Roy
National Microelectronics Research Centre
"Lee Maltings"
Prospect Row, Cork, Ireland
Email: terence.odonnell@nmrc.ie

***Abstract*— High-current, low-voltage power converters with fast transient response are needed for powering digital systems such as microprocessors. Microfabricated coupled inductors for such power converters are discussed. A four-phase microfabricated magnetic structure with 14 nH of inductance per phase has been fabricated for a 5 MHz, 5 V-to-1 V, 10 A dc-dc converter. The first prototype devices have been built with nickel-iron (NiFe) cores and copper conductors on a silicon substrate. Small-signal measurements on the inductors have been performed and predictions have been confirmed. A model for analyzing the performance of coupled inductors is presented. The devices have been implemented in a prototype converter and the measured performance is compared with the predicted results.**

I. Introduction

High-current, low-voltage power converters with fast transient response are needed for powering digital systems such as microprocessors which are projected to require 100 A or more at under 1 V [1]. The challenge in this application is that the load current can step from near zero to full load or vice versa in a matter of nanoseconds, and the voltage must be held stable throughout the step, with a projected tolerance of less than 50 mV [1]. The combination of high current and fast response requires a voltage regulator module (VRM) located immediately adjacent to the load. The VRM must be small in size, have high efficiency and extremely fast response. Microfabricated inductors [2]-[8] are attractive solutions towards addressing these requirements as they provide a means of integrating and miniaturizing the inductor.

In a buck converter with a load-current step, the output capacitor supplies (or sinks) the immediate difference in current while the inductor current is ramped up or down to match the new load current. A small inductor allows ramping the current quickly to minimize the output capacitor requirement but that approach can lead to large ripple currents and thus high losses. One strategy is to use high frequency to reduce this ripple, but the high frequency leads to high switching and gate-drive losses.

Using coupled inductors can help the designer bypass these tradeoffs. In [12], [13] it was shown that coupling the inductors in a two-phase interleaved converter can reduce ripple currents. A topology using three gapped legs was introduced. Based on that work, [14], [15], [16] show a different gapping configuration for two-phase converters which leads to higher ripple reduction. Additionally, a topology that allows practical operation with strong coupling and with more than two phases was introduced. The result was significant performance improvements; the ripple current in the inductors and the MOSFETs could be reduced without degrading the transient response time [14], [15], [16].

Based on the above mentioned work we have designed, fabricated and implemented a microfabricated coupled inductor integrated with a 5 MHz, 5 V-to-1 V converter designed for a maximum load current of 10 A. The microfabricated coupled inductors offer the benefit of having small inductors capable of operating at high frequencies and also enhancing performance by coupling. These are the first such structures to be integrated onto a silicon substrate thus providing scope for implementation with on-chip integrated power converters for microprocessors.

II. Principle of Operation

For the purpose of explaining the basic principle of coupled inductors, we discuss only a two-phase system in this section. The basic topology of a two-phased coupled inductor is shown in Fig. 1. The two phase inductors L_1 and L_2 are coupled together and the mutual inductance M represents the coupling effect between the two inductors. The dots, placed as shown in Fig. 1, indicate a negative value of M for the voltage polarities shown.

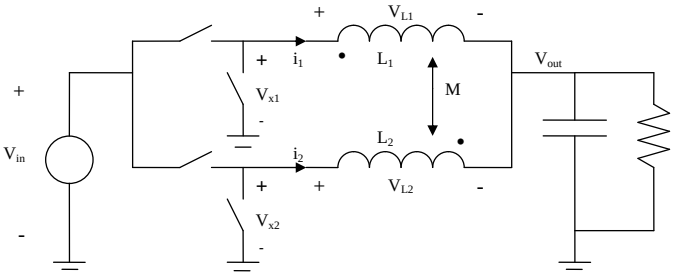

Fig. 1. Two-phase buck converter with coupled inductors.

The voltages applied across the two corresponding windings are related to the currents by [12]:

$$v_{L1} = L_1 \frac{di_1}{dt} + M \frac{di_2}{dt} \tag{1}$$

$$v_{L2} = L_2 \frac{di_2}{dt} + M \frac{di_1}{dt} \tag{2}$$

One can see that the current slope of one inductor is affected by the voltage across the other inductor; as shown in [12], [13], [14], [15], [16], the result is reduced ripple current. Assuming

0-7803-8399-0/04/$20.00 ©2004 IEEE.

the self-inductances of both phases, L_1 and L_2, are equal to a value L, we can define the coupling factor as follows:

$$\alpha = \frac{M}{L} \tag{3}$$

If we wish to analyze the effect of coupling factor on ripple, it is important to first consider which other parameter(s) will be held fixed. In [13], [14], [15], the leakage inductance is held constant in order to keep the transient response constant, and it is shown that increasing α as high as possible minimizes ripple. The ratio of ripple with coupling to the ripple without coupling, based on holding the leakage inductances, and thus the energy storage, fixed is given by [12]

$$\frac{\Delta i_{L,coup}}{\Delta i_{L,uncoup}} = \frac{1+\alpha\frac{D}{1-D}}{1-\alpha} \tag{4}$$

where D is the duty cycle of each phase of the converter. Note that α is between -1 and 0 because M is negative. Uncoupled inductors correspond to $\alpha = 0$. The coupling effect gets stronger as the absolute value of α increases, and thus the current ripple is reduced. The smallest ripple can be achieved when there is perfect coupling (α = -1). In practice perfect coupling can not be realized, but the highest practical value of α gives the best ripple reduction.

To use the advantages of coupled inductors in a converter with any number of phases, [14], [15] introduced a "ladder core" inductor topology. This topology affords strong coupling for multi-phase inductors, which cannot be achieved with other topologies, as confirmed by the review of possible multi-phase coupling topologies in [17].

III. Model Formulation

A ladder core topology [4] can be constructed as shown in Fig. 2. In [14], the equivalent magnetic circuit shown in Fig. 2 is developed to analyze the behavior of the ladder core structure. In the magnetic circuit, $\mathcal{R}_l$ is the leakage reluctance, $\mathcal{R}_{tb}$ is the sum of the reluctances of top and bottom outer legs across any one window, and $\mathcal{R}_u$ is the reluctance of the rung of the ladder, which is also the post around which the wire is wound. Each MMF source corresponds to a winding, with a value Ni equal to the product of the current i and number of turns N in the corresponding winding [14].

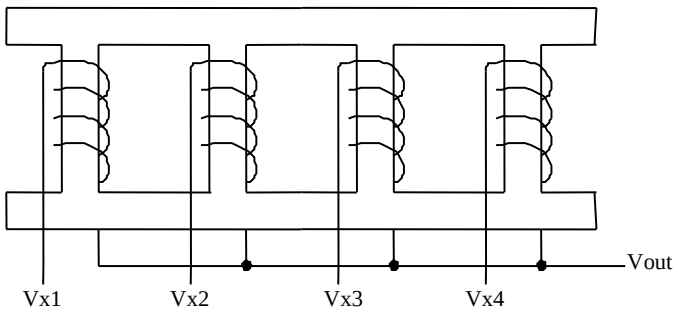

Fig. 2. Ladder core topology [14]

Based on Fig. 3 [14] writes

$$\Phi_u = \mathbf{A}\mathcal{F}, \tag{5}$$

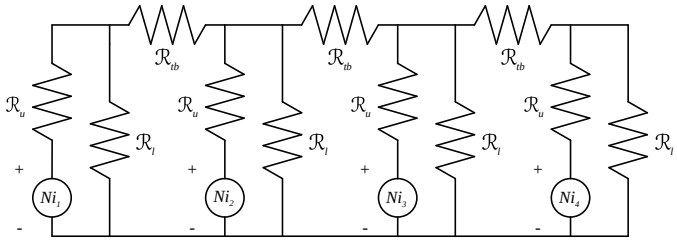

Fig. 3. Magnetic circuit model for four-phase coupled inductor. From [14].

where Φ_u is a vector containing the magnetic flux in each rung of the ladder structure, $\mathcal{F}$ is a vector of the MMF values at each node at the top of Fig. 3, and, for four phases,

$$\mathbf{A} = \begin{bmatrix} \frac{1}{\mathcal{R}_{tb}}+\frac{1}{\mathcal{R}_\ell} & -\frac{1}{\mathcal{R}_{tb}} & 0 & 0 \\ -\frac{1}{\mathcal{R}_{tb}} & \frac{2}{\mathcal{R}_{tb}}+\frac{1}{\mathcal{R}_\ell} & -\frac{1}{\mathcal{R}_{tb}} & 0 \\ 0 & -\frac{1}{\mathcal{R}_{tb}} & \frac{2}{\mathcal{R}_{tb}}+\frac{1}{\mathcal{R}_\ell} & -\frac{1}{\mathcal{R}_{tb}} \\ 0 & 0 & -\frac{1}{\mathcal{R}_{tb}} & \frac{1}{\mathcal{R}_{tb}}+\frac{1}{\mathcal{R}_\ell} \end{bmatrix}, \tag{6}$$

The matrix $\mathbf{A}$ may be similarly expressed for any number of phases. From

$$\Phi_u = \frac{Ni - \mathcal{F}}{\mathcal{R}_u}, \tag{7}$$

an expression for the vector of currents in each winding as a function of the vector of flux in each rung can be found. [14]

$$i = \frac{1}{N}(\mathcal{R}_u + A^{-1})\Phi_u \tag{8}$$

where i is a vector containing the currents in each winding.

The magnetic flux waveforms and current waveforms are calculated using the model derived above. Both waveforms have dc components and ac components which are calculated separately.

The dc components are calculated by assuming that the dc currents in each phase are equal [14]. This is necessary for proper operation, and may be achieved by the same active or passive methods that are used for uncoupled multi-phase converters. Thus, with total current in the load I_{total} and n phases, the dc component of current in each phase is $I_{phase,dc} = I_{total}/n$. The dc component of flux in the outside legs of the ladder core (top and bottom in Fig. 2) is zero and the flux in each rung is [14]

$$\Phi_{u,dc} = \frac{NI_{phase,dc}}{\mathcal{R}_u + \mathcal{R}_\ell}. \tag{9}$$

The voltage across each winding will switch from $V_{in} - V_{out}$ to $-V_{out}$. The relationship between the flux change in the rung and the voltage is [14]

$$V = -N\frac{d\Phi_u}{dt} \tag{10}$$

From the duty cycle and the period, (10) can be used to obtain the ac component of flux in the rung, and from equation (8), the ac components the winding currents can be calculated [14]. The ac component of the MMF $\mathcal{F}$ can be found by inverting (5); the MMF can then be used to calculate flux in the outside legs of the ladder core (top and bottom in Fig. 2) using [14]

$$\Phi_{tb} = \frac{\Delta\mathcal{F}}{\mathcal{R}_{tb}}. \tag{11}$$

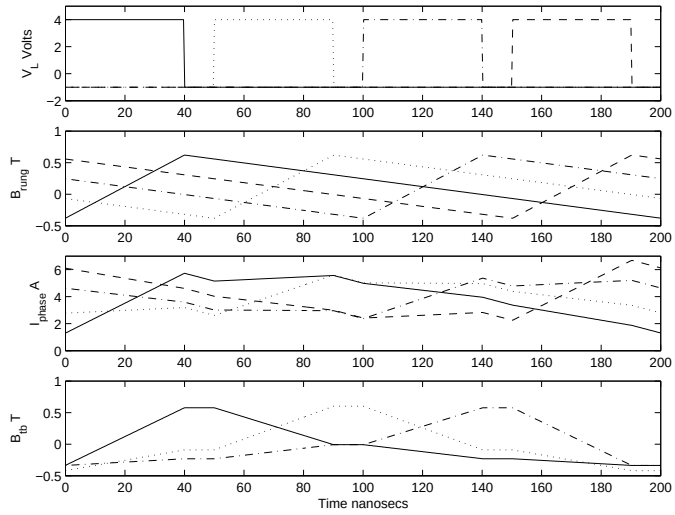

Fig. 4. Simulated results for a four-phase 5 V-to-1 V, 5 MHz converter operated at 4 A dc output current.

Now we have all the components of fluxes and currents. Example waveforms are shown in Fig. 4 for the first four-phase microfabricated coupled inductor-based 5 MHz, 5 V-to-1 V converter (described in Section VII).

IV. Fabrication

Fig. 5, Fig. 6 and Fig. 7 show the layout and cross-section of the microfabricated coupled inductors. The device consists of four rectangular NiFe cores and four single-turn copper windings. The layout is such that each winding lies under two rectangular cores. Fig. 6 shows eight conductors belonging to the four windings of copper. Similar shades represent the same winding with each half under separate cores. The cores are shown by four large rectangles in Fig. 6. The vertical sidewalls of the cores correspond to the vertical rungs of the ladder structure shown in Fig. 2. The direction of the dc currents in each winding is also shown in Fig. 6. Fig. 7 is a micrograph of one such core and respective halves of two windings from one of the fabricated devices.

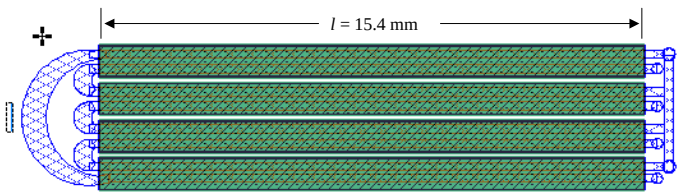

Fig. 5. Layout of the microfabricated coupled inductors

Fig. 6. Schematic of the cross-sectional view of the microfabricated coupled inductors. Eight conductors constitute four single-turn windings, each represented by a similar shade. The four larger rectangles represent the cores. The direction of the conductor dc current into the plane of the page is shown by an X and out of the plane of the paper is shown by a ●.

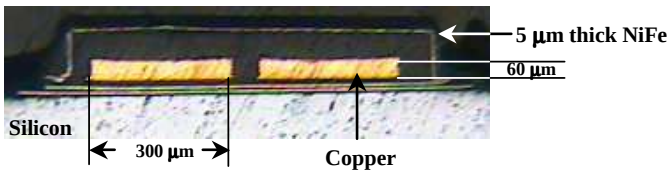

Fig. 7. Micrograph of one core section surrounding conductors belonging to two separate phases.

TABLE I

Specifications for core ($Ni_{45}Fe_{55}$) and windings (copper)
Saturation flux density: 1.5 T
Coercivity: 2 Oe
Relative permeability ($Ni_{45}Fe_{55}$): 300
Resistivity ($Ni_{45}Fe_{55}$): 50 $\mu\Omega$-cm
Core thickness: 5 μm per layer
Copper thickness: 60 μm

The fabrication process is detailed in [4]; we provide a brief description here. The basic structure consists of a racetrack shaped copper winding sandwiched between two layers of magnetic material. A silicon substrate is coated with a 3 μm thick layer of insulation (BCB - Benzocyclobutane) upon which a layer of magnetic material (alloy of NiFe, 45% nickel, 55% iron) is electroplated using a pulse reverse plating technique. The electroplating is done using a Ti/Cu seed layer on a mould formed by a patterned photoresist (AZ 9260). After plating, the photoresist and seed layer are stripped. To insulate the magnetic layer from the copper windings, a layer of SU8 epoxy type photoresist is spun on and patterned. The copper windings are then electroplated, again using a Ti/Cu seed layer. The mould for electroplating is formed using the AZ 9260 photoresist. The thickness of the electroplated copper is 60 μm. The windings are then covered by a layer of SU8, to isolate them from the top magnetic layer. The top magnetic layer is electroplated in a manner similar to the first layer of magnetic material. However in order to form the mould for the top, a layer of an electrophoretic resist is used. The electrophoretic resist allows the mould to be formed evenly on the vertical sidewalls and hence no vias are required to connect the top magnetic layer to the bottom. The material specifications for the devices are listed in Table I. Our first prototypes have one layer of NiFe cores; we are presently processing another batch of devices with two layers of NiFe cores.

V. Design of Coupled Inductor Geometry

The design goal was to build a 5 MHz, 5 V-to-1 V multi-phase, 10 A, dc-dc converter with a per-phase inductance of 14 nH. For a fixed output voltage of 1 V, we calculate that a per-phase dc current of 2.5 A will maintain the maximum loss due to dc resistance at 5% of output power. The dimensions of the device that were calculated to satisfy the inductance requirement and power loss specification are shown in Fig. 5 and Fig 7. For each phase in the coupled structure, with number of turns (N) equal to one, two layers of core each having a thickness t of 5 μm, saturation flux density of B_{sat} of 1.5 T, the length l was calculated to be 15.4 mm to maintain

flux swings within the saturation limits of the core. For ease of fabrication, we decided to have only one turn for each winding for our preliminary designs.

VI. Small-Signal Tests

The first prototypes have been fabricated with only one layer of magnetic core. The results we report in this paper are all for devices with a single layer of core. Small-signal measurements have been performed on the first prototypes. We physically shorted the windings of the two phases shown in Fig. 7 and performed small-signal measurements across them using a four wire measurement with an impedance analyzer (Agilent 4192A). This test measures the inductance of due leakage flux in the air gap that exists between the windings and that due to energy stored in a skin depth along the inside edges of the windings (the edges in the center of Fig. 7). We predict 14 nH per phase at 5 MHz; Fig. 8 confirms our predictions within 2 nH of our prediction at 5 MHz.

We performed a second test on another device fabricated using the same process run as that used in the first test. The two ends of each of the phase windings were probed, while maintaining the other phases open, to observe the symmetry in the structure. Finite element analysis was used to accurately capture the electromagnetic configuration of this setup to predict an inductance of 45 nH at 5 MHz for three phases. The measurements for each of these phases (curves A-C in Fig. 8) correlate closely to the simulated result. The fourth phase has copper looping through cores that are not adjacent to each other (the outermost conductors in Fig. 6) and hence was expected to have larger measured inductances than the other three phases. This can be seen in the measured result (curve D in Fig. 8). These results confirm that the phases exhibit very similar characteristics.

The ac resistance of the device was also measured at 5 MHz. We performed this measurement after integrating the device with the prototype board which is shown in Fig. 10 in order to include the ac resistance of each phase of the device, the associated bond wires used for connecting the device to the board, the interconnect on the board and that of the 14 μF chip capacitors soldered between the output terminals of the inductor and the ground plane. The terminals of each phase were probed while maintaining an open circuit in the other terminals. Fig. 9 shows the measured ac resistance of two phases of the device. A maximum measured resistance of 370 mΩ (R_{ac}) per phase was observed at 5 MHz. This value represents the per-phase ac loss component of the output section of the circuit board at 5 MHz. The dc resistance (R_{dc}) of this configuration was measured to be 40 mΩ per phase.

VII. 5 MHz DC-DC converter

The microfabricated coupled inductors were integrated with a prototype 5 V-1 V, 10 A DC-DC converter designed to operate at 5 MHz. The prototype board consisted of printed circuit board with four copper layers each 70 μm thick separated by 200 μm. Four commercial PWM ICs and a silicon die consisting of four coupled inductors were assembled on the board. Each phase of the converter was operated at 5 MHz and was designed to carry a peak current of 2.5 A. Fig. 10

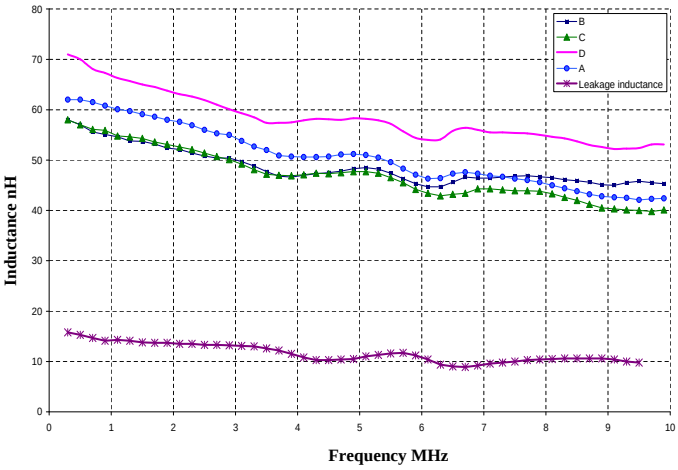

Fig. 8. Inductance from small-signal measurements performed on the microfabricated coupled inductors

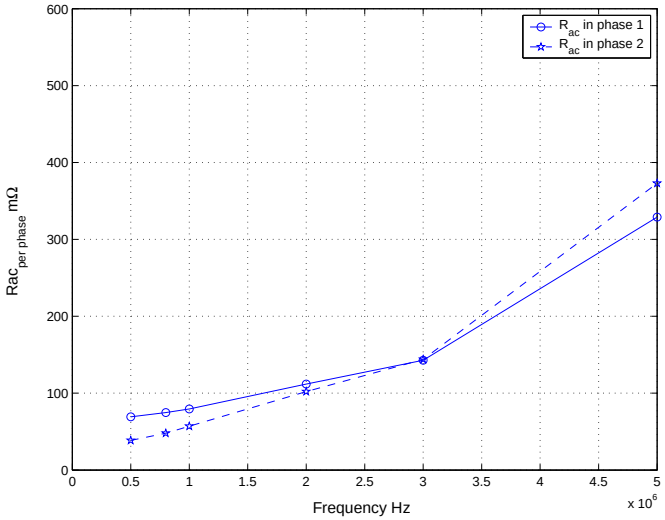

Fig. 9. R_{ac} from small-signal measurements performed on the microfabricated coupled inductors after integrating with test circuit.

shows a photograph of the prototype circuit board that was used for the experimental results. The bond wires connecting the inductors to the board add a stray inductance of 6 nH (estimated by finite element analysis). The specifications of the converter are listed in Table II.

VIII. Electrical Measurements

Experiments on the 4 phase dc-dc converter were performed to convert 5 V dc at the input to 1 V dc at the output. Each phase was activated by a 5 MHz PWM signal with 20% duty cycle. The four 40 ns pulses corresponding to the on times of each phase were spaced apart from each other by 10 ns

TABLE II

Electrical specifications of DC-DC converter
5 V (V_{in}) to 1 V (V_{out})
5 MHz per phase operating frequency
10 A rated dc output current (I_{out})

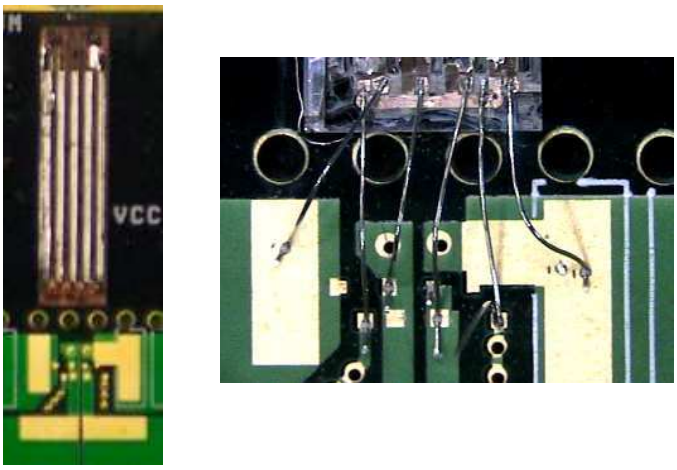

Fig. 10. Photograph of the microfabricated coupled inductor on the prototype dc-dc converter. The silicon die consisting of the four-phase microfabricated coupled inductor is shown with the bond-wire interconnects on the right.

(Fig. 4). An external load consisting of a bank of resistors was used to vary the output current. The output voltage was maintained at 1 V by adjusting the duty cycle. All duty cycles were varied simultaneously to ensure that the voltage at the output terminals of each inductor was at 1 V. We performed experiments with a separate power supply for the gate-drive circuitry and did not include the associated loss in efficiency calculations, since it was optimized for a lower frequency of operation than 5 MHz. The results of our initial experiments are shown in Fig. 11. Our initial experiments are limited to a maximum dc output current of 4 A. The 120 μm-diameter aluminum bond wires used to connect to the inductors to the board may not handle currents as high as 10 A. We intend to make more measurements (discussed below) at the existing current limit before operating the converter at higher currents. Measured results are plotted in Fig. 11 and are compared with predictions in Section IX.

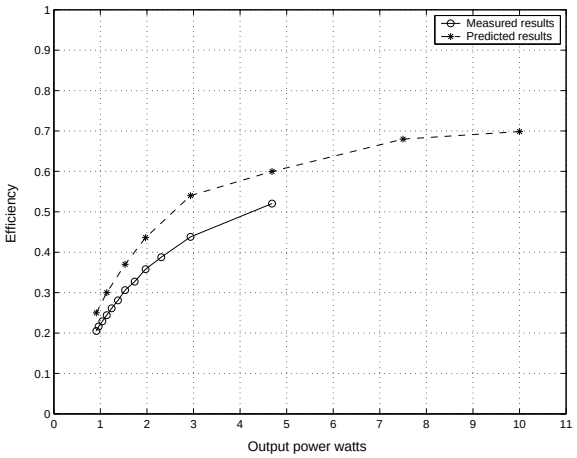

Fig. 11. Measured and predicted results of a four-phase 5 V-to-1 V, 5 MHz converter with microfabricated coupled inductors.

It is difficult to measure phase current without adding any stray inductance and changing the current waveforms. We plan to measure the current by measuring the voltage drop across a sense resistor placed in series with the inductors between the V_x node and the positive terminal of the inductor (see Fig. 1). Our initial tests had a 5 mΩ sense resistor in each of the phases. The power loss across these resistors was small compared to that of the inductors. However, the switching noise at the V_x node (Fig. 1) was too high to allow an accurate voltage measurement across such small values. To improve the signal-to-noise ratio, we plan to use 500 mΩ resistors temporarily soldered in just for the ripple current measurement.

IX. Predicted performance

The model described in Fig. 3 was used to predict the performance of the converter at various load currents. The conductor dc losses are calculated from the dc resistance. The conductor ac loss at each frequency is calculated using a Fourier series representation of the current waveform. We used a discrete Fourier transform function to extract the harmonic components of the inductor ripple current shown in Fig. 4. The ac resistance of the conductors was calculated in a skin depth of copper at each frequency. The core eddy-current loss was also calculated as a Fourier series representation of the ac flux waveform shown in Fig. 4 using techniques described in [18], [19]. Hysteresis loss was estimated from coercivity and ac flux amplitude. Hysteresis loss is insensitive to frequency and is non-linear and hence cannot be computed by Fourier analysis. The predicted results include the dc resistance and ac resistances of the aluminum bond-wire interconnects (19 mΩ and 30 mΩ at 5 MHz respectively) and a net leakage inductance of 20 nH which includes parasitic inductance due to the bond wires. Predicted results are shown in Fig. 11.

The theoretical predictions and the measured results match within a maximum difference of 25%. The model described in Fig 3 is an accurate model for a similar coupled inductor topology described in [14]. This model was considered to be an approximation of the electromagnetic configuration in the microfabricated coupled inductors. We attribute discrepancies in efficiency to the lack of a refined model for these preliminary devices. Other possible causes could be the losses in the parasitics in the board and conduction losses in gate-drive circuitry. The performance analysis does not include the gate-drive power.

The measurement of current waveforms to observe ripple reduction has not been performed. In order to demonstrate that performance enhancement is achieved due to magnetic material in the coupled inductor structure, we simulated the performance of a device with the exact same cross-section as shown in Fig. 6 using finite element analysis, except that the cores were removed. The per-phase inductance of the structure was determined to be 6 nH. The inductance due to the bond wires is 6 nH. With a total inductance of approximately 12 nH per phase a 5 V-1 V, 5 MHz converter would have a peak-to-peak inductor ripple current of nearly 14 A in each phase. Fig. 4 shows a per-phase peak-to-peak ripple of nearly 5 A — about three times smaller than what would flow through the inductor compared to the same structure with no core. Should the core have had no contribution towards coupling

we would have measured drastically lower efficiencies. The moderate measured efficiencies indicate otherwise. This is a rough indication that the magnetic material has an important role in determining the performance of the device.

The low measured efficiencies are not surprising. These devices were based on several design constraints mostly related to fabrication. For example, the copper conductors were limited to a height of 60 μm by a process constraint. With respect to the electrical performance, taller conductors could improve efficiency by reducing conductor ac and dc losses. Also, our first prototypes had only one layer of core and not two as originally planned. Please note that our predictions are based on one core. Adding another layer could enhance coupling factor, thus causing greater ripple current cancellation and could also reduce the ac flux density in the core. The above considerations also present the trade-off between improving conductor losses at the expense of worsening magnetic losses by adding more magnetic material. A thorough design optimization such as that performed in [14] would be required to investigate such trade-offs. Such an optimization has not been performed. We plan to perform such an optimization and then fabricate another batch of inductors with better performance.

X. Conclusion

The design goal was to build a 5 MHz, 5 V-to-1 V four-phase, 10 A, dc-dc converter with a per-phase inductance of 14 nH for fast transient response. A 5 MHz, 5 V-to-1 V dc-dc four-phase converter has been designed and tested up to 4 A. We have demonstrated a working power converter. Measured results have been compared with predictions. The measurements reported in this paper are valuable towards designing a new batch of microfabricated coupled inductors and a new converter with better performance. The functionality of the circuit has been demonstrated up to a peak dc current of 4 A — a step closer towards realizing practical low voltage, high current voltage regulator modules with microfabricated inductors.

Acknowledgment

The authors thank Ningning Wang, Stephen O'Reilly, Paddy Byrnes and Kenneth Rodgers at the National Microelectronics Research Centre, Cork, Ireland. This work was supported by Intel Corporation and The Dartmouth Nanomagnetics Initiative funded by the National Institute of Standards and Technology.

References

[1] B. Rose, "Voltage regulator technology requirements," in *4th Annual Intel technology Symposium*, Sept. 1990.

[2] K. H. Kim, J. Kim, H. J. Kim, S. H. Han, and H. J. Kim, "A megahertz switching DC/DC converter using FeBN thin film inductor," *IEEE Transactions on Magnetics*, vol. 38, pp. 3162–3164, Sept. 2002.

[3] J. Boggetto, Y. Lembeye, J. Ferrieux, and J. Keradec, "Microfabricated power inductors on silicon," in *33rd Annual Power Electronics Specialists Conf.*, 2002.

[4] M. Brunet, T. O'Donnell, J. O'Brien, P. McCloskey, and C. O'Mathuna, "Design study and fabrication techniques for high power density microtransformers," in *16th Annual IEEE Applied Power Electronics Conference and Exposition*, pp. 1189–1195, 2001.

[5] M. Allen, J. Y. Park, J.-W. Park, and Y.-H. Joung;, "Fabrication of high current and low profile micromachined inductor with laminated Ni/Fe core," *IEEE Transactions on Magnetics*, vol. 25, no. 1, pp. 106–111, 2002.

[6] M. Edo, M. Gekinozu, Z. Hayashi, Y. Katayama, K. Kuroki, K. Matsuzaki, H. Nakazawa, S. Sugahara, and E. Yonezawa, "Micro DC-DC converter that integrates planar inductor on power IC," *IEEE Transactions on Magnetics*, vol. 36, no. 5, pp. 3518–3521, 2000.

[7] V. Korenivski and R. B. van Dover, "Design of high frequency inductors based on magnetic films," *IEEE Transactions on Magnetics*, vol. 34, no. 4, pp. 1375–1377, 1998.

[8] M. Xy, T. M. Liakopoulos, C. H. Ahn, S. H. Han, and H. J. Kim, "A microfabricated transformer for high-frequency power or signal conversion," *IEEE Transactions on Magnetics*, vol. 34, no. 4, pp. 1369–1371, 1998.

[9] Y. Sasaki, S. Morita, T. Hatanai, A. Makino, T. Sato, and K. Yamasawa, "High frequency soft magnetic properties of nanocrystallien Fe-(Co)-Hf-O films with high electrical resistivity and their applicationto micro DC-DC converter," *NanoStructured Materials*, vol. 8, no. 8, pp. 1025–1032, 1997.

[10] M. Mino, K. Tsukamoto, K. Yanagisawa, A. Tago, and T. Yachi, "A compact buck-converter using a thin-film inductor," in *Proceedings of Applied Power Electronics Conference, APEC'96*, pp. 422–426, Mar. 1996.

[11] C. R. Sullivan and S. R. Sanders, "Measured performance of a high-power-density microfabricated transformer in a DC-DC converter," in *27th Annual Power Electronics Specialists Conf.*, vol. 1, pp. 287–294, June 1996.

[12] P.-L. Wong, P. Xu, P. Yang, and F. Lee, "Investigating coupling inductors in the interleaving QSW VRM," in *IEEE Applied Power Electronics Conference*, pp. 973–978, Mar. 2000.

[13] P.-L. Wong, P. Xu, P. Yang, and F. Lee, "Performance improvements of interleaving VRMs with coupling inductors," *IEEE Transactions on Power Electronics*, vol. 16, no. 4, p. 499507, 2001.

[14] J. Li, C. R. Sullivan, and A. Schultz, "Coupled-inductor design optimization for fast-response low-voltage dc-dc converters," in *17th Annual IEEE Applied Power Electronics Conference and Exposition*, 2002.

[15] A. M. Schultz and C. Sullivan, "Voltage converter with coupled inductive windings, and associated methods, U.S. Patent number 6,362,986, Volterra Semiconductor Corp," 2002.

[16] J. Li, A. Stratakos, and A. Schultz, "Using coupled inductors to enhance transient performance of multi-phase buck converters," in *19th Annual IEEE Applied Power Electronics Conference and Exposition*, 2004.

[17] P. Zumel, O. Garca, J. Cobos, and J. Uceda, "Magnetic integration for interleaved converters," in *IEEE Applied Power Electronics Conference*, 2002.

[18] E. C. Snelling, *Soft Ferrites, Properties and Applications*. Butterworths, second ed., 1988.

[19] G. J. Mehas, K. D. Coonley, and C. R. Sullivan, "Design of microfabricated inductors for microprocessor power delivery," in *IEEE Applied Power Electronics Conference*, pp. 1181–1187, Mar. 1999.